ACS APPLIED MATERIALS & INTERFACES

www.acsami.org Research Article

Boosting the Efficiency of NiO_x-Based Perovskite Light-Emitting Diodes by Interface Engineering

Haoran Wang, Hao Yuan, Jiahao Yu, Chen Zhang, Kang Li, Mengqing You, Wenqiang Li, Jian Shao, Jun Wei, Xiaoyu Zhang, Rui Chen,* Xuyong Yang,* and Weiwei Zhao*

Cite This: *ACS Appl. Mater. Interfaces* 2020, 12, 53528−53536 Read Online

ACCESS | Metrics & More | Article Recommendations | Supporting Information

ABSTRACT: Nickel oxide (NiO_x) is a promising hole-transporting material for perovskite light-emitting diodes (PeLEDs) because of its low cost, excellent stability, and simple fabrication process. However, the electroluminescence efficiencies of NiO_x-based PeLEDs are greatly limited by inefficient hole injection and exciton quenching at the NiO_x−perovskite interfaces. Here, a novel interfacial engineering method with sodium dodecyl sulfate-oxygen plasma (SDS-OP) is demonstrated to simultaneously overcome the aforementioned issues. Experimental results reveal that a short OP treatment on the top of the SDS-coated NiO_x significantly deepens the NiO_x work function (from 4.23 to 4.85 eV) because of the formation of a large surface dipole, allowing for efficient hole injection. Moreover, the SDS-OP layer passivates the electronic surface trap states of perovskite films and suppresses the exciton quenching by NiO_x. These improvements inhibit the nonradiative decays at the NiO_x−perovskite interface. As a result, the external quantum efficiency of $CsPbBr_3$ LEDs is increased from 0.052 to 2.5%; that of $FAPbBr_3$ nanocrystals LEDs is increased from 5.6 to 7.6%.

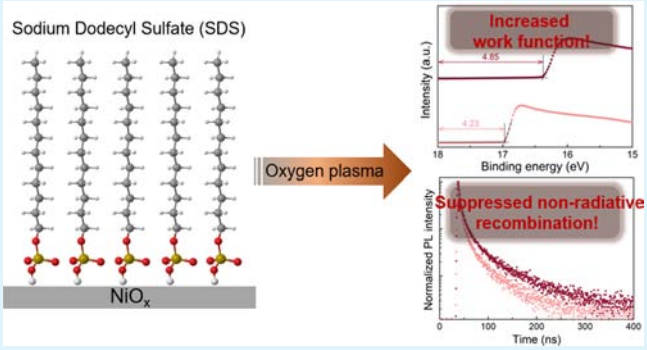

KEYWORDS: *perovskite, NiO_x, electroluminescence, interface, SDS, PeLEDs*

INTRODUCTION

Solution-processed metal halide perovskites have emerged as a promising class of materials for light-emitting diodes (LEDs) because of their superb optoelectronic properties such as high carrier mobility,[1,2] high color purity, and easy color tunability.[3−7] With the evolution of perovskite synthesis[7−11] and device architectures,[4,12,13] device performances have been significantly improved in the past several years. Recently, using perovskite LEDs (PeLEDs) with green, red, and near-infrared emissions, impressive external quantum efficiencies (EQEs) beyond 20% have been achieved,[14−20] making them comparable to the most advanced organic LEDs and quantum-dot LEDs.

Currently, the most popular p-type material used to construct a PeLED is poly(3,4-ethylenedioxythiophene):polystyrene sulfonate (PEDOT:PSS).[4−8,11−14,17] However, PEDOT:PSS with high acidity can severely etch the indium tin oxide (ITO) anode, thereby resulting in the release of In and Sn atoms. The released In and Sn atoms, known to be exciton-quenching sites, can diffuse into the perovskite layer and accelerate the degradation of PeLEDs,[21] posing a significant threat to the long-term stability of the devices. Inorganic p-type semiconductors such as carbon quantum dots,[22] NiO_x,[23−35] and copper sulfide−gallium−tin oxide[36] are alternative hole-transporting materials for perovskite-based LEDs owing to their excellent carrier mobility, high transmittancy, and good chemical and physical stability. Among them, NiO_x is particularly attractive because of its p-type characteristics with a wide band gap and easy electronic structure tunability as well as good electron-blocking ability. Recently, Lee and coworkers fabricated high-quality perovskite emitters through compositional, dimensional, and interfacial modulations, and have demonstrated NiO_x-based PeLEDs with a maximum EQE of 14.6% and improved operational stability,[33] revealing the potential of NiO_x films as hole-transporting materials for-high performance PeLEDs. However, some fundamental issues from the device perspective are still lingering. For example, previous studies on NiO_x-based PeLEDs were focused mainly on the perovskite film processing and its relevant material design.[27,33,37] Careful modification of the NiO_x−perovskite interface and its effect on electroluminescence remain largely unexplored. The previously reported NiO_x-based perovskite photovoltaics have been verified that the surface traps at the NiO_x−perovskite interface can not only quench photoluminescence (PL)

Received: September 7, 2020
Accepted: November 4, 2020
Published: November 12, 2020

https://dx.doi.org/10.1021/acsami.0c16139
ACS Appl. Mater. Interfaces 2020, 12, 53528−53536

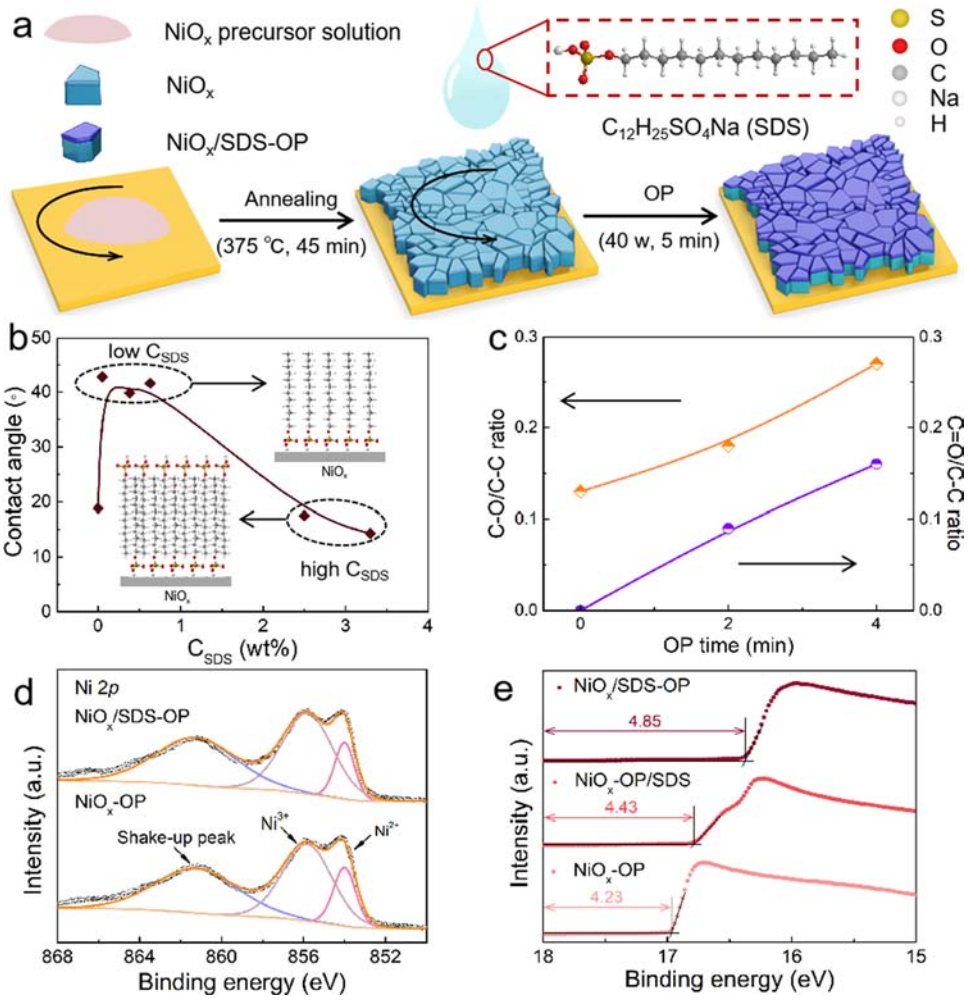

Figure 1. (a) Schematic illustration showing the NiO_x/SDS-OP film fabrication procedure. (b) Contact angle (CA) measurements for glass/NiO_x and glass/SDS-coated NiO_x. Inset in (b) shows the SDS structures at the NiO_x interface at different C_{SDS}. (c) Statistical C−O/C−C and C═O/C−C ratios calculated from the XPS data. (d) XPS spectra of the NiO_x-OP and NiO_x/SDS-OP films for Ni 2p. (e) UPS spectra of NiO_x-OP, NiO_x-OP/SDS, and NiO_x/SDS-OP films.

emission but also impair the crystallinity and stability of the perovskite layer.[26,29] In addition, there is a large energy level mismatch at the NiO_x−perovskite interface, which has a detrimental impact on the radiative recombination rate and thus the device performance.[28] Therefore, controlling the NiO_x−perovskite interface properties aimed on efficient hole injection and preservation of superior emissive in perovskite films can be an effective way to improve the device efficiency.

Herein, a novel interfacial method based on sodium dodecyl sulfate-oxygen plasma (SDS-OP) is introduced to improve the NiO_x−perovskite interface properties via a short OP treatment on the top of the SDS-coated NiO_x. A combined X-ray and ultraviolet photoelectron spectroscopy (XPS and UPS) analysis reveals that the SDS-OP interfacial layer induces the formation of a large surface dipole because of the synergistic effect of SDS layer dipoles and the increase in the concentration of N^{3+} species. This results in a significant increase in the work function (from 4.23 to 4.85 eV) of NiO_x and a reduction of the energy offset between NiO_x and perovskites (from 0.69 to 0.38 eV), which effectively facilitates the hole injection. Besides, the introduction of the SDS-OP layer passivates the electronic surface trap states of perovskite films and suppresses the exciton quenching by NiO_x as confirmed by XPS, transient absorption (TA), and PL lifetime measurements. These two advantages are efficient to inhibit the mass nonradiative recombination at the NiO_x−perovskite interface. As a result, these improvements boost the EQE of $CsPbBr_3$ LEDs from 0.052 to 2.5%; that of the $FAPbBr_3$ nanocrystal LED from 5.6 to 7.6%.

RESULTS AND DISCUSSION

The preparation procedure of the NiO_x/SDS-oxygen plasma (SDS-OP) film is schematically shown in Figure 1a. Typically, the NiO_x precursor solution was prepared by mixing nickel acetate tetrahydrate and monoethanolamine in ethanol.[38] Then, the prepared precursor solution was spin coated on an ITO substrate followed by thermal annealing. After cooling to room temperature, a solution of SDS (unless specially mentioned, the SDS concentration (C_{SDS}) is 0.38 wt %) was spin coated on the NiO_x film, and the as-prepared SDS-coated NiO_x film was treated with a short OP (see more details in the Experimental Methods section). The elemental maps of the NiO_x/SDS-OP films in Figure S1 show homogeneous distribution of S and Na, indicating that the SDS-OP is uniformly present on the NiO_x film.

Because of the coexistence of a hydrophobic alkyl chain and hydrophilic sulfate group in the SDS's chemical structure, SDS

https://dx.doi.org/10.1021/acsami.0c16139
ACS Appl. Mater. Interfaces 2020, 12, 53528−53536

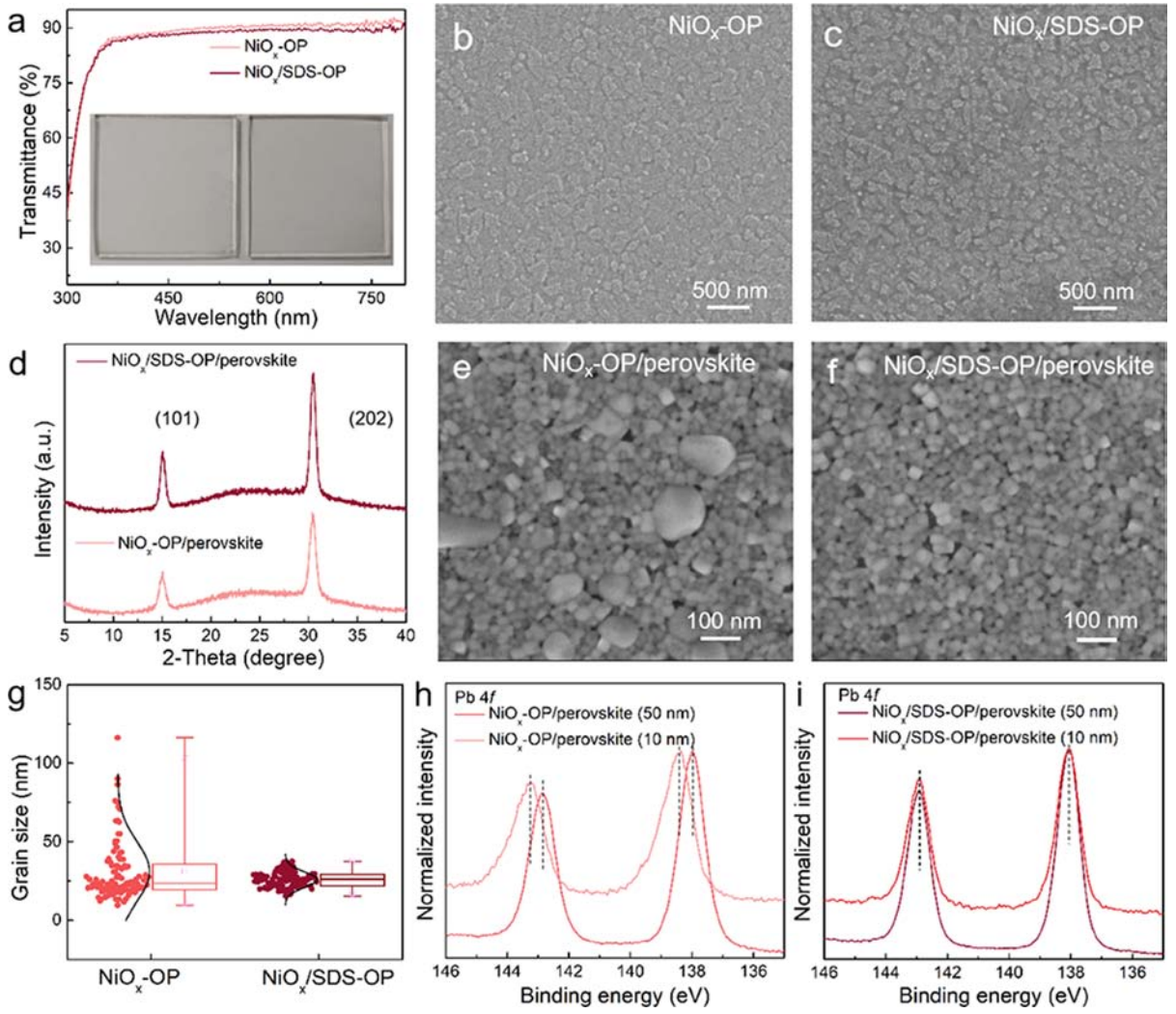

Figure 2. (a) Transmittance spectra of the NiO_x-OP and NiO_x/SDS-OP films coated on the quartz substrate. The FE-SEM images of (b) NiO_x-OP and (c) NiO_x/SDS-OP films. (d) X-ray diffraction (XRD) patterns, (e,f) FE-SEM images and (g) grain size distribution of perovskite films deposited on ITO/NiO_x-OP and ITO/NiO_x/SDS-OP substrates. Pb 4f XPS spectra of the perovskite film (10 or 50 nm) deposited on (h) ITO/NiO_x-OP and (i) ITO/NiO_x/SDS-OP substrates.

can provide selective interfacial contacts with both NiO_x and perovskite layers. This is confirmed by the variation in the CA of the SDS-coated NiO_x film at different C_{SDS}. As depicted in Figures S2 and 1b, the SDS-coated NiO_x films show the CA greater than 39° at low C_{SDS}, which is less hydrophilic than the NiO_x surface with a CA of 19°. Such an obvious increment in the CA is attributed to the interaction between sulfonate groups of SDS and NiO_x by electrostatic force, resulting in a hydrophobic alkyl chain pointing to air side and thus reducing the wettability of the NiO_x surface.[39,40] However, this situation could be reversed through a hydrophobic interaction at higher C_{SDS}, leaving the hydrophilic sulfate groups exposed to air. After the OP treatment, the surface energy of the SDS (low C_{SDS})-coated NiO_x films decreased leading to a CA of <22° (Figure S3); this implies an increased polarity of SDS, which is because of the presence of polar oxygen-containing functional groups on the surface as a result of the oxidation of the SDS carbon chain toward the air side. To verify this, and to study the impact of SDS-OP on the chemical state of the NiO_x film, XPS characterization was performed. In the C 1s spectra (Figure S4), the components at 284.8, 286.4, and 288.7 eV refer, respectively, to C−C, C−O, and C═O bonds.[41,42] Note that the proportion of C−O and C═O is significantly increased after OP treatment. The integrated peak area ratio of C−O/C−C is calculated to be 0.13, 0.18, and 0.27, and that of C═O/C−C is calculated to be 0, 0.09, and 0.16 as the OP treatment time increases from 0, 2, to 4 min, respectively (Figure 1c). The C═O-functionalized SDS plays a critical role in suppressing nonradiative recombination at the NiO_x−perovskite interface (as will be discussed later). Figure 1d shows the Ni 2p spectra of the NiO_x-OP and NiO_x/SDS-OP films. Both samples exhibit three dominant peaks located at 854.1, 855.9, and 861.3 eV, corresponding to the NiO, Ni_2O_3, and the shake-up process of NiO_x, respectively.[24] The obtained Ni^{3+}/Ni^{2+} ratio for the NiO_x-OP film is calculated to be 3.08, which is nearly identical to that for the NiO_x-OP/SDS films (3.02) (Figure S5), but lower than that for the NiO_x/SDS-OP film (3.81). Because the Ni^{3+} state (occurring in Ni_2O_3) generates p-type conductivity in the NiO_x film, the higher Ni^{3+}/Ni^{2+} ratio in the NiO_x/SDS-OP film would be conducive to the increase of hole conductivity.[31,43] The reason for the higher concentration of Ni^{3+} can be well understood as follows. Plasma ablation of some atoms in the SDS layer will generate free Na^+ ions. These ions are accelerated to high energy by the plasma sheath potential and doped into the

https://dx.doi.org/10.1021/acsami.0c16139
ACS Appl. Mater. Interfaces 2020, 12, 53528−53536

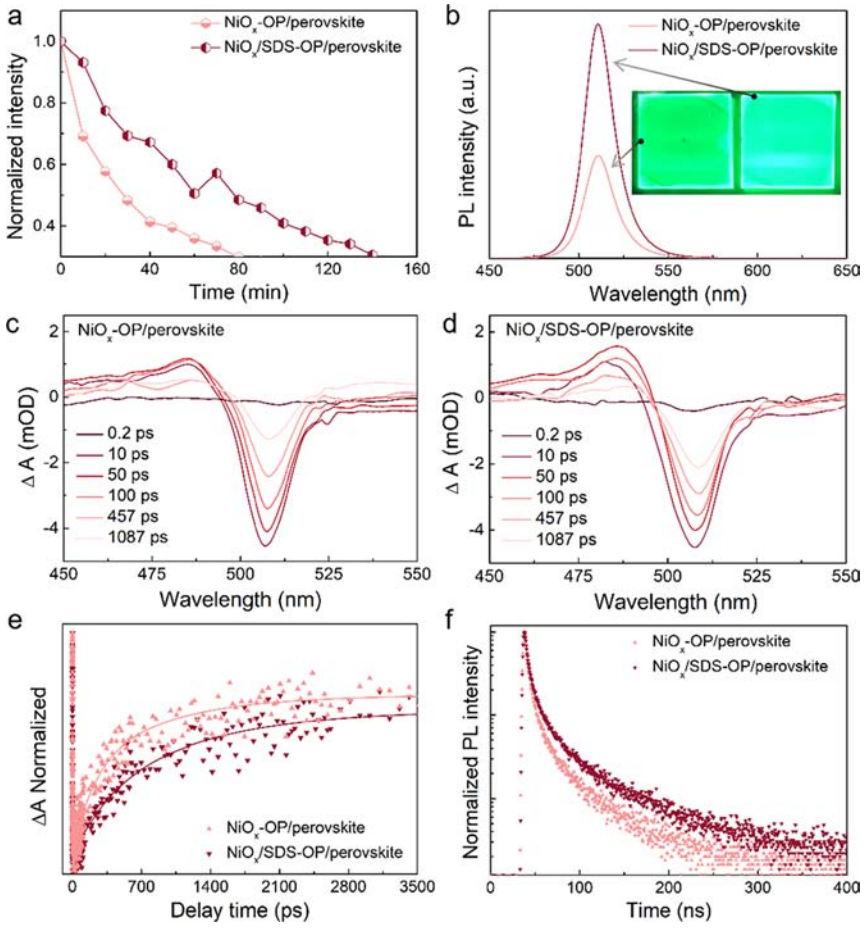

Figure 3. (a) Photostability in air, (b) steady-state PL, (c−e) TA, and (f) time-resolved photoluminescence (TRPL) spectra of the quartz/NiO_x-OP/perovskite and quartz/NiO_x/SDS-OP/perovskite films. Inset in (b) shows the fluorescence photograph of perovskite films under UV illumination.

NiO lattice.[44,45] To achieve charge neutrality, a Ni^{3+} should be formed for every Na^+ introduced, thereby increasing the Ni^{3+} concentration.

UPS was taken to evaluate the effect of SDS-OP on the energy level of the NiO_x film (Figure 1e). It can be found that after the SDS modification, the work function of NiO_x-OP is increased from 4.23 to 4.43 eV, which is because of the formation of a molecular dipole moment by the SDS layer (Figure S6). In the case of NiO_x/SDS-OP, owing to the contribution of the synergistic effect of SDS layer dipoles and the increase in concentration of Ni^{3+} species, the work function is significantly increased to 4.85 eV. This deepening of work function would lead to more favorable energy level alignment between the valence band maximum (VBM) of the perovskite emitter (Figures S7−S9 and Table S1), which benefits efficient hole injection. Moreover, the energy of valence-band edge relative to the Fermi level is 0.86 eV for the NiO_x/SDS-OP film, which is lower than that of NiO_x-OP (1.17 eV) (Figure S10). The reduced energy demonstrates a more net p-type NiO_x/SDS-OP, which is very consistent with the result from the Ni 2p XPS. Furthermore, the NiO_x/SDS-OP film shows excellent resistance to organic solvents. As shown in Figure S11 and Table S2, the VBM of the NiO_x/SDS-OP film is nearly identical after dimethyl sulfoxide (DMSO) and chlorobenzene wash, suggesting its promising future for solution-processed optoelectronic devices.

Optical transmittance spectra (Figure 2a) show that both NiO_x-OP and NiO_x/SDS-OP films on glass exhibit high transparency in the visible range, with the average transmittance over 89% within the wavelength range of 400−800 nm. The field-emission scanning electron microscopy (FE-SEM) images of both NiO_x-OP and NiO_x/SDS-OP films demonstrate similar surface morphologies (Figure 2b,c). The corresponding atomic force microscopy (AFM) images in Figure S12 illustrate that the root mean square roughness is reduced from 2.72 nm for the NiO_x-OP film to 2.49 nm for the NiO_x/SDS-OP film, indicating that SDS-OP treatment is effective in planarizing the NiO_x surface. The smoother surfaces can provide a better contact with the perovskite layer, which benefits the device performance.

The perovskite films were deposited on NiO_x-OP and NiO_x/SDS-OP substrates by one-step spin coating a CsBr/BABr/$PbBr_2$/PEO precursor solution from DMSO (see more details in the Experimental Methods section). XRD patterns of both samples exhibit two peaks at 15.0 and 30.5°, corresponding to the (101) and (202) planes of the $CsPbBr_3$ perovskite orthorhombic phase, respectively.[13] Notably, the intensity of (101) and (202) peaks for the perovskite film on the NiO_x/SDS-OP is much higher than that on the NiO_x-OP, suggesting a better $CsPbBr_3$ perovskite crystallinity with SDS-OP treatment. The high crystallinity for the perovskite film is very beneficial to high fluorescence emission[46,47] and crystal stability.[48] The top-view FE-SEM images in Figure 2e,f indicate that the perovskite film on the NiO_x/SDS-OP is smoother than that on the NiO_x-OP. The corresponding grain size distributions are shown in Figure 2g. The grain size distribution of the $CsPbBr_3$ perovskite film on the NiO_x/SDS-OP is uniform, while that on the NiO_x-OP is broadly distributed from 10 to 116 nm.

https://dx.doi.org/10.1021/acsami.0c16139
ACS Appl. Mater. Interfaces 2020, 12, 53528−53536

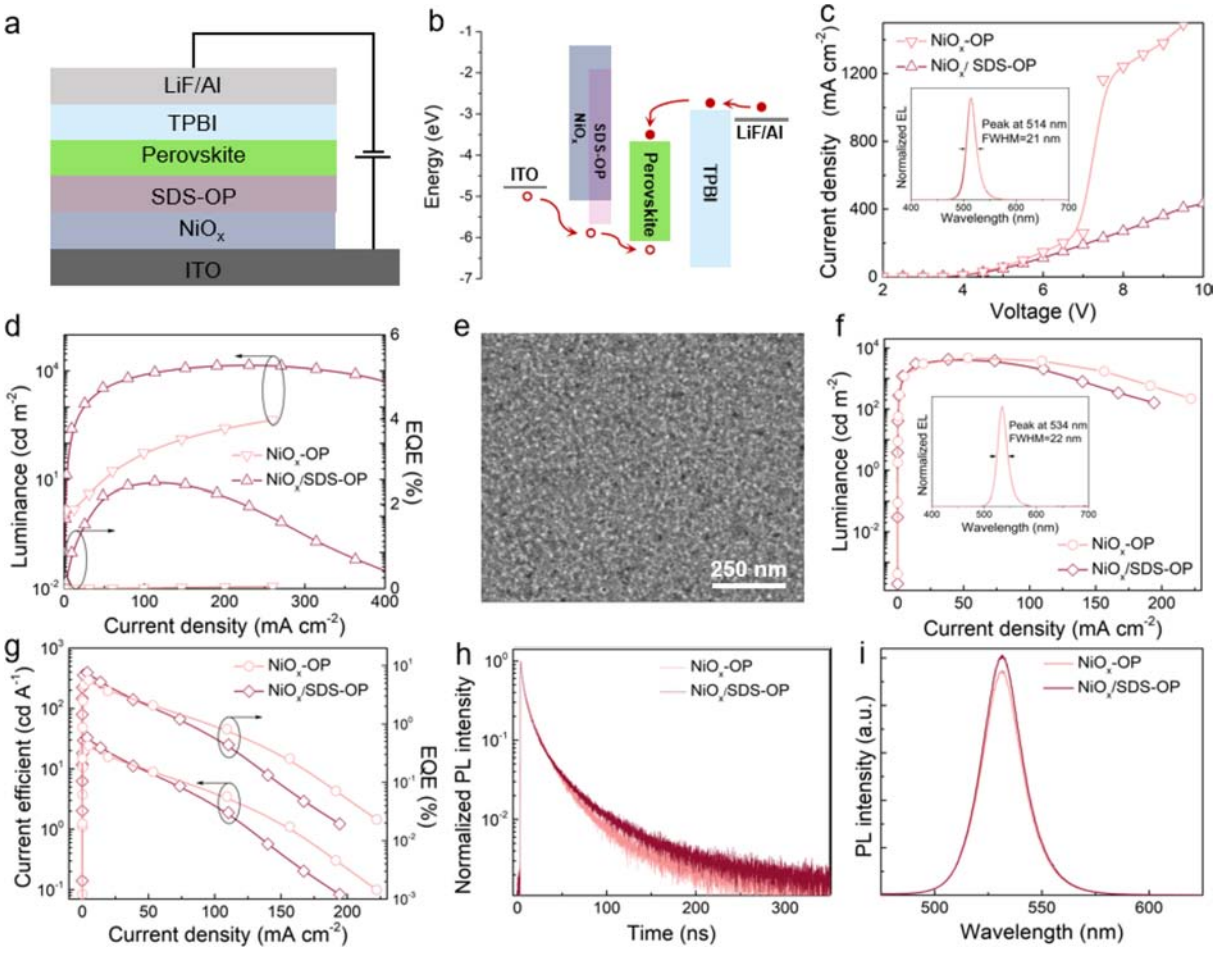

Figure 4. (a) Device structure and (b) energy level diagram of the $CsPbBr_3$ LEDs. (c) $J-V$ and (d) $L-J-$EQE curves of $CsPbBr_3$ LEDs with NiO_x-OP and NiO_x/SDS-OP. Inset in (c) shows the electroluminescent (EL) spectra of $CsPbBr_3$ LED with NiO_x-OP and NiO_x/SDS-OP. (e) FE-SEM image of the $FAPbBr_3$ NC film. (f) $L-J$ and (g) current efficiency (CE)$-J-$EQE curves of $FAPbBr_3$ LEDs with NiO_x-OP and NiO_x/SDS-OP. Inset in (f) shows the EL spectra of $FAPbBr_3$ LED with NiO_x-OP and NiO_x/SDS-OP. (h) TRPL and (i) steady-state PL spectra of the quartz/NiO_x-OP/poly (N,N′-bis(4-butylphenyl)-N,N′-bis(phenyl)-benzidine) (poly-TPD)/$FAPbBr_3$ NCs and quartz/NiO_x/SDS-OP/poly-TPD/$FAPbBr_3$ NC films.

To better understand the effect of SDS-OP on the perovskite crystal growth and the resulting interfacial properties, XPS analysis was performed. 50- and 10 nm-thick perovskite films were deposited on the NiO_x-OP and NiO_x/SDS-OP substrates to investigate bulk-like (thick films) and interface (thin films) characteristics, respectively.[49] The Pb 4f spectra for both 50 nm-thick perovskite films exhibit similar dominant peaks at 138.0 and 142.9 eV, which can be indexed to the Pb $4f_{7/2}$ and Pb $4f_{5/2}$ levels, respectively. For the 10 nm-thick perovskite film formed on the NiO_x-OP substrate, however, a shift of the Pb 4f peaks to a higher binding energy (BE) can be clearly seen, indicating an electron-deficient chemical state of the Pb atoms possibly because of the existence of halide vacancy defects. Those trap states located at the interface could induce severe nonradiative recombination and accelerate the degradation of the perovskite, resulting in a short PL lifetime and poor stability, which are detrimental to PeLED performance. In contrast, there is no obvious Pb 4*f* BE shift in the NiO_x/SDS-OP/perovskite (10 nm-thick), demonstrating that the interface defects are effectively passivated when introducing the C═O-functionalized SDS-OP that acts as Lewis bases for defect-healing by interacting with uncoordinated Pb^{2+}. This similar chemical environment allows the crystals to grow similarly at the interface and in bulk films, thus leading to uniform grain size distribution. Furthermore, the improved interface properties between the perovskite and NiO_x with SDS-OP are advantageous to enhance the stability of perovskite films. As shown in Figure 3a, the relative PL intensity of the NiO_x-OP/perovskite is strongly decreased after continuous UV irradiation under ambient conditions for 80 min, retaining only 30% of its initial value, while that of the NiO_x/SDS-OP/perovskite keeps 48% of its original emission intensity.

Steady-state PL measurements were carried out to further study the influence of SDS-OP on the optical properties of perovskite films. On contact with NiO_x-OP coated substrates, the perovskite films show much weaker PL intensities (Figure S13), which is attributed to exciton quenching caused by the traps and charge transfer at the NiO_x-perovskite interface. After introduction of SDS-OP, a considerable increase of PL intensity is observed, which can be readily seen in the inset of Figure 3b, suggesting that the radiative recombination in perovskite films formed on the NiO_x/SDS-OP substrate is enhanced. Note that owing to the more compatible energy level of the SDS-OP-treated NiO_x with the VBM of the perovskite, the SDS-OP would induce faster charge transfer favoring PL quenching. Therefore, the improved emission should be ascribed to the reduction of trap-states by SDS-OP instead of the suppression of charge transfer.

https://dx.doi.org/10.1021/acsami.0c16139
ACS Appl. Mater. Interfaces 2020, 12, 53528−53536

TA measurements were conducted to further reveal the suppressed nonradiative recombination at the NiO_x−perovskite interface (Figure 3c−e). Both TA spectra show an identical sharp negative signal at 512 nm, corresponding to the excitonic bleach. It can be seen that the dynamic of bleach recovery for NiO_x/SDS-OP/perovskite is much slower, namely 52.1% decrease of ΔA at 1087 ps as compared to 71.4% that for the NiO_x-OP/perovskite. Because ΔA is proportional to the exciton density at the lowest excited states, the slowed bleach recovery kinetics indicate that the excitons are less likely to be charged by NiO_x and trapped at perovskite surface defects. The fitted kinetics for NiO_x/SDS-OP/perovskite was 1010.48 ps, which is 1.3-fold longer than that for NiO_x-OP/perovskite (757.24 ps) (Figure 3e and Table S3). Such a longer exciton lifetime further confirms the increased probability of radiative recombination in the perovskite film formed on the NiO_x/SDS-OP substrate. Furthermore, the PL decay of NiO_x/SDS-OP/perovskite (average PL lifetime of 60.14 ns) is slower than that of NiO_x-OP/perovskite (41.54 ns) as shown in Figure 3f and Table S4, also supporting the conclusion that nonradiative process was suppressed upon SDS-OP modification.

We then tested how the increased work function and the suppressed nonradiative recombination influence the LED performance. Figure 4a presents the device structure consisting ITO as the anode, SDS-OP-coated NiO_x (20 nm) as the hole-transport layer, the $CsPbBr_3$ perovskite (50 nm), 1,3,5-tris(1-phenyl-1H-benzimidazol-2-yl)benzene (TPBI, 40 nm) as the electron-transport layer, and LiF (1 nm)/Al (100 nm) as the cathode. The corresponding energy level diagram of the device in Figure 4b shows that electrons can easily inject from the LiF/Al cathode and transport to the $CsPbBr_3$ perovskite emissive layer via the lowest unoccupied molecular orbital of TPBI. However, owing to the high energy barrier (~0.7 eV) from the VBM of NiO_x-OP to the $CsPbBr_3$ perovskite, hole injection is relatively difficult. Once we increase the work function by ~0.6 eV and downshift the corresponding VBM level by ~ 0.3 eV for NiO_x with SDS-OP, the energy barrier is reduced and thus effectively improves hole injection. This prediction is consistent with the electrical characterization results (Figure S14), which shows that the hole injection current in the device is increased after using SDS-OP.

The J−V characteristics show a decrease in current density for the device with NiO_x/SDS-OP (Figure 4c), which could be attributed to the insulation nature of SDS-OP. The EL spectra of both samples given in the inset of Figure 4c exhibit an emission peak at 514 nm, with a narrow full width half-maximum (fwhm) of 21 nm. Figure 4d presents the L−J−EQE curves of $CsPbBr_3$ LED based on NiO_x-OP and NiO_x/SDS-OP. The turn-on voltage (3.2 V) of the device with NiO_x/SDS-OP is lower than that of the device with NiO_x-OP (4.3 V), reconfirming that SDS-OP improves the hole injection into the emissive layer. The peak luminance (14,456 cd m^{-2}) of the PeLED with NiO_x/SDS-OP is 32.8 times higher than that of the one with NiO_x-OP (441 cd m^{-2}). The maximum EQE (2.5%) of the device based on NiO_x/SDS-OP is much higher than that of the one based on NiO_x-OP (0.052%). Moreover, PeLEDs with NiO_x/SDS-OP display a half-life time of ≈0.79 h at an initial brightness of 100 cd m^{-2} (Figure S15), which is a 13.5-fold increase as compared to that of devices using conventional PEDOT:PSS (0.058 h). Thus, these results demonstrate the advantage of the SDS-OP in fabricating PeLEDs with high performance and stability.

$FAPbBr_3$ nanocrystals (the SEM image of its thin film shown in Figure 4e) were chosen as emitters to further explore the advantage of SDS-OP in NiO_x-based PeLEDs. The device architecture consists of layers of ITO/SDS-OP-coated NiO_x (20 nm)/poly-TPD (20 nm)/$FAPbBr_3$ (20 nm)/TPBI (40 nm)/LiF (1 nm)/Al (100 nm). Figure 4f,g compares the L−J and CE−J−EQE characteristics of $FAPbBr_3$ LEDs based on NiO_x-OP and NiO_x/SDS-OP. The maximum luminance is 4754 cd m^{-2} for the device with NiO_x-OP and 4282 cd m^{-2} for the one with NiO_x/SDS-OP. The inset in Figure 4f shows the EL spectra of both samples, which show an emission peak at 534 nm, with a narrow fwhm of 22 nm and exhibits no contribution from the charge transport materials. The peak CE and EQE of the $FAPbBr_3$ LED with NiO_x-OP reach 24.2 cd A^{-1} and 5.6%, respectively, while $FAPbBr_3$ LEDs with NiO_x/SDS-OP show a substantially improved light-emitting efficiency, with a peak CE of 32.8 cd A^{-1} and a maximum EQE of 7.6%.

We examined the TRPL and PL spectra of the $FAPbBr_3$ NCs films formed on the two types of substrates. As shown in Figure 4h and Table S5, the PL lifetime of the $FAPbBr_3$ films deposited on NiO_x/SDS-OP/poly-TPD (43.98 ns) is longer than that of the $FAPbBr_3$ NCs films deposited on NiO_x-OP/poly-TPD (31.18 ns). The PL spectra shown in Figure 4i follow the same trend as their PL lifetimes. These results indicate that the exciton quenching by NiO_x is still significant despite the insertion of a 20 nm-thick poly-TPD layer between NiO_x and $FAPbBr_3$, and this long-range exciton quenching that is detrimental to the device performance can be effectively suppressed after using SDS-OP. We thus suggest that in addition to the deepened work function for efficient hole injection, the exciton quenching caused by NiO_x should be paid special attention.

CONCLUSIONS

In summary, we demonstrated a novel interfacial engineering method with SDS-OP that achieves efficient NiO_x-based PeLEDs. The easy-processed SDS-OP layer plays multiple roles in boosting the device efficiency. It helps to enhance the hole injection ability, passivate the electronic surface trap states of perovskite films, and suppress the exciton quenching by NiO_x. As a consequence of all these beneficial improvements, the EQE of $CsPbBr_3$ LEDs is increased from 0.052 to 2.5%; that of $FAPbBr_3$ nanocrystal LED is increased from 5.6 to 7.6%. We believe these findings would offer important interfacial design insights to improve the efficiency of solution-processed oxide-based PeLEDs.

EXPERIMENTAL METHODS

Materials. Nickel acetate tetrahydrate (99.995%), DMSO (anhydrous, 99.9%), CsBr (99.999%), $PbBr_2$ (99.999%), FA-acetate (FAAc, 99%), OA (90%), and PEO (average M_v 100,000) were purchased from Sigma-Aldrich. SDS (99%) was purchased from Alfa Aesar. Ethanol (AR, ≥99.7%), chlorobenzene (AR, ≥99.5%), $Pb(acetate)_2{\cdot}3H_2O$ ($Pb(Ac)_2{\cdot}3H_2O$, AR, ≥99.5%), octane (CP, ≥98%), ethyl acetate (EA, AR, ≥99.5%), and hexane (AR, ≥97%) were purchased from Sinopharm Chemical Reagent. OAmBr (99.5%) and BABr (≥99.5%) were purchased from Xi'an p-led. Poly-TPD was purchased from American Dye Source. TPBI (>99%) and LiF were purchased from Lumtec. All of the materials were used as received.

NiO*x* Precursor Solution. The nickel acetate tetrahydrate (0.25 mmol) and monoethanolamine (15 μL) were dissolved in anhydrous ethanol (2.5 mL). Mixtures were stirred with a temperature of 60 °C for 4 h and then at room temperature one night. The NiO_x precursor solution was filtered with 0.45 μm polytetrafluoroethylene filters before use.

Perovskite Precursor Solutions. $PbBr_2$, CsBr, and BABr were dissolved in DMSO with a ratio of 1:1.2:0.4 as the precursor of

https://dx.doi.org/10.1021/acsami.0c16139
ACS Appl. Mater. Interfaces 2020, 12, 53528−53536

perovskite, with a concentration of 100 mg mL^{-1}, and then 0.3 wt % of PEO was added to improve the morphology of the film. The solution was stirred with a temperature of 60 °C overnight and filtered with 0.45 μm polytetrafluoroethylene filters before use.

Synthesis and Purification of $FAPbBr_3$ NCs. 76 mg $Pb(Ac)_2 \cdot 3H_2O$, 78 mg FAAc, 210 mg OAmBr, 2 mL dried OA, and 8 mL octane were mixed in a 25 mL beaker, followed by tip-ultrasonication with a power of 35 W for 1 min. After completion of the reaction, adding EA (30 mL) into the crude solution and centrifuging at 7500 rpm for 5 min, the obtained precipitate was dissolved in hexane (2 mL). To remove the unreacted precursors, the solution was centrifuged at 7500 rpm for 1 min. The $FAPbBr_3$ NCs were precipitated again with the addition of EA (6 mL). These were finally redispersed in hexane (6 mg mL^{-1}).

Fabrication of $CsPbBr_3$ LED. Patterned ITO-coated glasses were ultrasonically cleaned with deionized water, acetone, and isopropyl alcohol for 15 min each, and treated with OP for 15 min before depositing the NiO_x films. NiO_x precursor solution was spin-cast onto the ITO substrates at 4000 rpm for 40 s and the film was annealed at 375 °C for 45 min in air. After cooling to room temperature, solutions of SDS (dissolved in ethanol at a concentration of 0.38 wt %) were spin coated onto the NiO_x layer at 4000 rpm for 40 s. Then, the ITO/NiO_x/SDS substrate was treated with OP at a power of 40 W for 5 min. The $CsPbBr_3$ perovskite film was deposited on the ITO/SDS-OP-coated NiO_x substrate at 4000 rpm for 40 s in a N_2-filled glove box, and annealed at 80 °C for 10 min. Finally, 40 nm of TPBI, 1 nm of LiF, and 100 nm of Al layers were sequentially deposited using a vacuum deposition clamber under a pressure below 4×10^{-4} Pa.

Fabrication of $FAPbBr_3$ NC LED. After fabrication of the SDS-OP-coated NiO_x films, these substrates were then transferred into a N_2-filled glove box, and a poly-TPD layer was deposited on the SDS-OP-coated NiO_x film using 8 mg ml^{-1} solution in chlorobenzene with a speed of 4000 rpm for 1 min, and the film was annealed at 150 °C for 20 min. The $FAPbBr_3$ layer was deposited on the ITO/SDS-OP-coated NiO_x/poly-TPD substrates using the $FAPbBr_3$ NC solution with a speed of 1500 rpm for 1 min. Finally, 40 nm of TPBI, 1 nm of LiF, and 100 nm of Al layers were sequentially deposited using a vacuum deposition clamber under a pressure below 4×10^{-4} Pa.

Characterization. AFM images were obtained using a Bruker Dimension Icon microscope. A field-emission scanning electron microscope (GeminiSEM 300 microscope) was used to acquire the film morphologies. XRD data were collected with a Bruker D8 Advance diffractometer. The steady-state PL and TRPL spectra were collected with an Edinburgh FLS920 PL spectrometer. The UPS and XPS were analyzed using a ThermoFisher ESCALAB 250Xi. TA spectra were obtained by using an ExciPro femtosecond TA pump−probe spectrometer (CDP Systems Corp). The electrical performance of the device was evaluated using a Keithley 2400 source meter and a PR-670 Spectra Colorimeter.

■ ASSOCIATED CONTENT

Supporting Information

The Supporting Information is available free of charge at https://pubs.acs.org/doi/10.1021/acsami.0c16139.

Elemental maps of the NiO_x/SDS-OP film, water CA of SDS-coated NiO_x, water CA of SDS-coated NiO_x treated with OP, C 1s XPS spectra of the SDS thin films treated with OP, XPS spectra of the NiO_x-OP/SDS films for Ni 2p, molecular dipole moment-induced change of the work function of the NiO_x film, Tauc plots, UPS spectra of the perovskite film, AFM images of NiOx-OP and NiOx/SDS-OP, steady-state PL spectra of quartz/perovskite and quartz/NiOx-OP/perovskite, J-V characteristics, operating lifetimes of the PeLEDs, energy levels of the perovskite films, summary of TA spectral fitting parameters, and summary of PL lifetime fitting parameters (PDF)

■ AUTHOR INFORMATION

Corresponding Authors

Rui Chen − *Department of Electrical and Electronic Engineering, Southern University of Science and Technology, Shenzhen, Guangdong 518055, China;* orcid.org/0000-0002-0445-7847; Email: chenr@sustech.edu.cn

Xuyong Yang − *Key Laboratory of Advanced Display and System Applications of Ministry of Education, Shanghai University, Shanghai 200072, China;* orcid.org/0000-0003-3597-1491; Email: yangxy@shu.edu.cn

Weiwei Zhao − *Flexible Printed Electronics Technology Center and State Key Laboratory of Advanced Welding & Joining, Harbin Institute of Technology, Shenzhen 518055, China;* orcid.org/0000-0002-0373-1146; Email: wzhao@hit.edu.cn

Authors

Haoran Wang − *Flexible Printed Electronics Technology Center and State Key Laboratory of Advanced Welding & Joining, Harbin Institute of Technology, Shenzhen 518055, China*

Hao Yuan − *Key Laboratory of Advanced Display and System Applications of Ministry of Education, Shanghai University, Shanghai 200072, China*

Jiahao Yu − *Department of Electrical and Electronic Engineering, Southern University of Science and Technology, Shenzhen, Guangdong 518055, China*

Chen Zhang − *Flexible Printed Electronics Technology Center and State Key Laboratory of Advanced Welding & Joining, Harbin Institute of Technology, Shenzhen 518055, China*

Kang Li − *Flexible Printed Electronics Technology Center and State Key Laboratory of Advanced Welding & Joining, Harbin Institute of Technology, Shenzhen 518055, China;* orcid.org/0000-0003-4600-2186

Mengqing You − *Key Laboratory of Advanced Display and System Applications of Ministry of Education, Shanghai University, Shanghai 200072, China*

Wenqiang Li − *Key Laboratory of Advanced Display and System Applications of Ministry of Education, Shanghai University, Shanghai 200072, China*

Jian Shao − *Flexible Printed Electronics Technology Center and State Key Laboratory of Advanced Welding & Joining, Harbin Institute of Technology, Shenzhen 518055, China;* orcid.org/0000-0003-0207-4858

Jun Wei − *Flexible Printed Electronics Technology Center and State Key Laboratory of Advanced Welding & Joining, Harbin Institute of Technology, Shenzhen 518055, China*

Xiaoyu Zhang − *College of Materials Science and Engineering, Jilin University, Changchun 130012, China;* orcid.org/0000-0001-7528-4405

Complete contact information is available at: https://pubs.acs.org/10.1021/acsami.0c16139

Author Contributions

H.W., H.Y., and W.L. fabricated and characterized the devices. M.Y. performed the transmittance and TRPL measurements. J.Y. and R.C. performed the TA measurements. H.W., J.Y., C.Z., K.L., J.S., J.W., X.Z., R.C., X.Y., and W.Z. analyzed and discussed the experimental results. H.W., H.Y., and J.Y. contributed equally to this work. All authors contributed to writing the article.

Notes

The authors declare no competing financial interest.

https://dx.doi.org/10.1021/acsami.0c16139
ACS Appl. Mater. Interfaces 2020, 12, 53528−53536

■ ACKNOWLEDGMENTS

This work was supported by Shenzhen Science and Technology Program (grant no. KQTD20170809110344233) and Bureau of Industry and Information Technology of Shenzhen through the Graphene Manufacturing Innovation Center (201901161514).

■ REFERENCES

(1) Wehrenfennig, C.; Eperon, G. E.; Johnston, M. B.; Snaith, H. J.; Herz, L. M. High Charge Carrier Mobilities and Lifetimes in Organolead Trihalide Perovskites. *Adv. Mater.* **2014**, *26*, 1584−1589.

(2) Shi, D.; Adinolfi, V.; Comin, R.; Yuan, M.; Alarousu, E.; Buin, A.; Chen, Y.; Hoogland, S.; Rothenberger, A.; Katsiev, K.; Losovyj, Y.; Zhang, X.; Dowben, P. A.; Mohammed, O. F.; Sargent, E. H.; Bakr, O. M. Low Trap-State Density and Long Carrier Diffusion in Organolead Trihalide Perovskite Single Crystals. *Science* **2015**, *347*, 519−522.

(3) Tan, Z.-K.; Moghaddam, R. S.; Lai, M. L.; Docampo, P.; Higler, R.; Deschler, F.; Price, M.; Sadhanala, A.; Pazos, L. M.; Credgington, D.; Hanusch, F.; Bein, T.; Snaith, H. J.; Friend, R. H. Bright Light-Emitting Diodes Based on Organometal Halide Perovskite. *Nat. Nanotech.* **2014**, *9*, 687−692.

(4) Cho, H.; Jeong, S.-H.; Park, M.-H.; Kim, Y.-H.; Wolf, C.; Lee, C.-L.; Heo, J. H.; Sadhanala, A.; Myoung, N.; Yoo, S.; Im, S. H.; Friend, R. H.; Lee, T.-W. Overcoming the Electroluminescence Efficiency Limitations of Perovskite Light-Emitting Diodes. *Science* **2015**, *350*, 1222−1225.

(5) Pan, J.; Shang, Y.; Yin, J.; De Bastiani, M.; Peng, W.; Dursun, I.; Sinatra, L.; El-Zohry, A. M.; Hedhili, M. N.; Emwas, A.-H.; Mohammed, O. F.; Ning, Z.; Bakr, O. M. Bidentate Ligand-Passivated $CsPbI_3$ Perovskite Nanocrystals for Stable Near-Unity Photoluminescence Quantum Yield and Efficient Red Light-Emitting Diodes. *J. Am. Chem. Soc.* **2018**, *140*, 562−565.

(6) Song, J.; Li, J.; Li, X.; Xu, L.; Dong, Y.; Zeng, H. Quantum Dot Light-Emitting Diodes Based on Inorganic Perovskite Cesium Lead Halides (CsPbX3). *Adv. Mater.* **2015**, *27*, 7162−7167.

(7) Wang, H.; Zhang, X.; Wu, Q.; Cao, F.; Yang, D.; Shang, Y.; Ning, Z.; Zhang, W.; Zheng, W.; Yan, Y.; Kershaw, S. V.; Zhang, L.; Rogach, A. L.; Yang, X. Trifluoroacetate Induced Small-Grained $CsPbBr_3$ Perovskite Films Result in Efficient and Stable Light-Emitting Devices. *Nat. Commun.* **2019**, *10*, 665.

(8) Song, J.; Fang, T.; Li, J.; Xu, L.; Zhang, F.; Han, B.; Shan, Q.; Zeng, H. Organic−Inorganic Hybrid Passivation Enables Perovskite QLEDs with an EQE of 16.48%. *Adv. Mater.* **2018**, *30*, 1805409.

(9) Zhang, X.; Lu, M.; Zhang, Y.; Wu, H.; Shen, X.; Zhang, W.; Zheng, W.; Colvin, V. L.; Yu, W. W. PbS Capped CsPbI3 Nanocrystals for Efficient and Stable Light-Emitting Devices Using p−i−n Structures. *ACS Cent. Sci.* **2018**, *4*, 1352−1359.

(10) Yuan, M.; Quan, L. N.; Comin, R.; Walters, G.; Sabatini, R.; Voznyy, O.; Hoogland, S.; Zhao, Y.; Beauregard, E. M.; Kanjanaboos, P.; Lu, Z.; Kim, D. H.; Sargent, E. H. Perovskite Energy Funnels for Efficient Light-Emitting Diodes. *Nat. Nanotech.* **2016**, *11*, 872−877.

(11) Jiang, Y.; Qin, C.; Cui, M.; He, T.; Liu, K.; Huang, Y.; Luo, M.; Zhang, L.; Xu, H.; Li, S.; Wei, J.; Liu, Z.; Wang, H.; Kim, G.-H.; Yuan, M.; Chen, J. Spectra Stable Blue Perovskite Light-Emitting Diodes. *Nat. Commun.* **2019**, *10*, 1868.

(12) Zhang, X.; Lin, H.; Huang, H.; Reckmeier, C.; Zhang, Y.; Choy, W. C. H.; Rogach, A. L. Enhancing the Brightness of Cesium Lead Halide Perovskite Nanocrystal Based Green Light-Emitting Devices through the Interface Engineering with Perfluorinated Ionomer. *Nano Lett.* **2016**, *16*, 1415−1420.

(13) Cho, H.; Wolf, C.; Kim, J. S.; Yun, H. J.; Bae, J. S.; Kim, H.; Heo, J.-M.; Ahn, S.; Lee, T.-W. High-Efficiency Solution-Processed Inorganic Metal Halide Perovskite Light-Emitting Diodes. *Adv. Mater.* **2017**, *29*, 1700579.

(14) Lin, K.; Xing, J.; Quan, L. N.; de Arquer, F. P. G.; Gong, X.; Lu, J.; Xie, L.; Zhao, W.; Zhang, D.; Yan, C.; Li, W.; Liu, X.; Lu, Y.; Kirman, J.; Sargent, E. H.; Xiong, Q.; Wei, Z. Perovskite Light-Emitting Diodes with External Quantum Efficiency Exceeding 20 Per cent. *Nature* **2018**, *562*, 245−248.

(15) Zhao, B.; Bai, S.; Kim, V.; Lamboll, R.; Shivanna, R.; Auras, F.; Richter, J. M.; Yang, L.; Dai, L.; Alsari, M.; She, X.-J.; Liang, L.; Zhang, J.; Lilliu, S.; Gao, P.; Snaith, H. J.; Wang, J.; Greenham, N. C.; Friend, R. H.; Di, D. High-Efficiency Perovskite−Polymer Bulk Heterostructure Light-Emitting Diodes. *Nat. Photonics* **2018**, *12*, 783−789.

(16) Cao, Y.; Wang, N.; Tian, H.; Guo, J.; Wei, Y.; Chen, H.; Miao, Y.; Zou, W.; Pan, K.; He, Y.; Cao, H.; Ke, Y.; Xu, M.; Wang, Y.; Yang, M.; Du, K.; Fu, Z.; Kong, D.; Dai, D.; Jin, Y.; Li, G.; Li, H.; Peng, Q.; Wang, J.; Huang, W. Perovskite Light-Emitting Diodes Based on Spontaneously Formed Submicrometre-Scale Structures. *Nature* **2018**, *562*, 249−253.

(17) Chiba, T.; Hayashi, Y.; Ebe, H.; Hoshi, K.; Sato, J.; Sato, S.; Pu, Y.-J.; Ohisa, S.; Kido, J. Anion-Exchange Red Perovskite Quantum Dots with Ammonium Iodine Salts for Highly Efficient Light-Emitting Devices. *Nat. Photonics* **2018**, *12*, 681−687.

(18) Zhao, X.; Tan, Z.-K. Large-Area Near-Infrared Perovskite Light-Emitting Diodes. *Nat. Photonics* **2020**, *14*, 215−218.

(19) Xu, W.; Hu, Q.; Bai, S.; Bao, C.; Miao, Y.; Yuan, Z.; Borzda, T.; Barker, A. J.; Tyukalova, E.; Hu, Z.; Kawecki, M.; Wang, H.; Yan, Z.; Liu, X.; Shi, X.; Uvdal, K.; Fahlman, M.; Zhang, W.; Duchamp, M.; Liu, J.-M.; Petrozza, A.; Wang, J.; Liu, L.-M.; Huang, W.; Gao, F. Rational Molecular Passivation for High-Performance Perovskite Light-Emitting Diodes. *Nat. Photonics* **2019**, *13*, 418−424.

(20) Fang, Z.; Chen, W.; Shi, Y.; Zhao, J.; Chu, S.; Zhang, J.; Xiao, Z. Dual Passivation of Perovskite Defects for Light-Emitting Diodes with External Quantum Efficiency Exceeding 20%. *Adv. Funct. Mater.* **2020**, *30*, 1909754.

(21) Cho, H.; Kim, Y.-H.; Wolf, C.; Lee, H.-D.; Lee, T.-W. Improving the Stability of Metal Halide Perovskite Materials and Light-Emitting Diodes. *Adv. Mater.* **2018**, *30*, 1704587.

(22) Wang, Z.; Yuan, F.; Sun, W.; Shi, H.; Hayat, T.; Alsaedi, A.; Fan, L.; Tan, Z. a. Multifunctional p-Type Carbon Quantum Dots: a Novel Hole Injection Layer for High-Performance Perovskite Light-Emitting Diodes with Significantly Enhanced Stability. *Adv. Opt. Mater.* **2019**, *7*, 1901299.

(23) Ren, Z.; Xiao, X.; Ma, R.; Lin, H.; Wang, K.; Sun, X. W.; Choy, W. C. H. Hole Transport Bilayer Structure for Quasi-2D Perovskite Based Blue Light-Emitting Diodes with High Brightness and Good Spectral Stability. *Adv. Funct. Mater.* **2019**, *29*, 1905339.

(24) You, J.; Meng, L.; Song, T.-B.; Guo, T.-F.; Yang, Y.; Chang, W.-H.; Hong, Z.; Chen, H.; Zhou, H.; Chen, Q.; Liu, Y.; De Marco, N.; Yang, Y. Improved Air Stability of Perovskite Solar Cells via Solution-Processed Metal Oxide Transport Layers. *Nat. Nanotech.* **2016**, *11*, 75−81.

(25) Boyd, C. C.; Shallcross, R. C.; Moot, T.; Kerner, R.; Bertoluzzi, L.; Onno, A.; Kavadiya, S.; Chosy, C.; Wolf, E. J.; Werner, J.; Raiford, J. A.; de Paula, C.; Palmstrom, A. F.; Yu, Z. J.; Berry, J. J.; Bent, S. F.; Holman, Z. C.; Luther, J. M.; Ratcliff, E. L.; Armstrong, N. R.; McGehee, M. D. Overcoming Redox Reactions at Perovskite-Nickel Oxide Interfaces to Boost Voltages in Perovskite Solar Cells. *Joule* **2020**, *4*, 1759−1775.

(26) Bai, Y.; Chen, H.; Xiao, S.; Xue, Q.; Zhang, T.; Zhu, Z.; Li, Q.; Hu, C.; Yang, Y.; Hu, Z.; Huang, F.; Wong, K. S.; Yip, H.-L.; Yang, S. Effects of a Molecular Monolayer Modification of NiO Nanocrystal Layer Surfaces on Perovskite Crystallization and Interface Contact toward Faster Hole Extraction and Higher Photovoltaic Performance. *Adv. Funct. Mater.* **2016**, *26*, 2950−2958.

(27) Chih, Y.-K.; Wang, J.-C.; Yang, R.-T.; Liu, C.-C.; Chang, Y.-C.; Fu, Y.-S.; Lai, W.-C.; Chen, P.; Wen, T.-C.; Huang, Y.-C.; Tsao, C.-S.; Guo, T.-F. NiO_x Electrode Interlayer and $CH_3NH_2/CH_3NH_3PbBr_3$ Interface Treatment to Markedly Advance Hybrid Perovskite-Based Light-Emitting Diodes. *Adv. Mater.* **2016**, *28*, 8687.

(28) Ji, W.; Liu, S.; Zhang, H.; Wang, R.; Xie, W.; Zhang, H. Ultrasonic Spray Processed, Highly Efficient All-Inorganic Quantum-Dot Light-Emitting Diodes. *ACS Photonics* **2017**, *4*, 1271−1278.

(29) Chen, W.; Zhou, Y.; Chen, G.; Wu, Y.; Tu, B.; Liu, F. Z.; Huang, L.; Ng, A. M. C.; Djurišić, A. B.; He, Z. Alkali Chlorides for the Suppression of the Interfacial Recombination in Inverted Planar Perovskite Solar Cells. *Adv. Energy Mater.* **2019**, *9*, 1803872.

(30) Liu, S.; Ho, S.; Chen, Y.; So, F. Passivation of Metal Oxide Surfaces for High-Performance Organic and Hybrid Optoelectronic Devices. *Chem. Mater.* **2015**, *27*, 2532−2539.
(31) Chen, W.; Liu, F.-Z.; Feng, X.-Y.; Djurišić, A. B.; Chan, W. K.; He, Z.-B. Cesium Doped NiO_x as an Efficient Hole Extraction Layer for Inverted Planar Perovskite Solar Cells. *Adv. Energy Mater.* **2017**, *7*, 1700722.
(32) Chen, W.; Zhou, Y.; Wang, L.; Wu, Y.; Tu, B.; Yu, B.; Liu, F.; Tam, H.-W.; Wang, G.; Djurišić, A. B.; Huang, L.; He, Z. Molecule-Doped Nickel Oxide: Verified Charge Transfer and Planar Inverted Mixed Cation Perovskite Solar Cell. *Adv. Mater.* **2018**, *30*, 1800515.
(33) Lee, S.; Kim, D. B.; Hamilton, I.; Daboczi, M.; Nam, Y. S.; Lee, B. R.; Zhao, B.; Jang, C. H.; Friend, R. H.; Kim, J.-S.; Song, M. H. Control of Interface Defects for Efficient and Stable Quasi-2D Perovskite Light-Emitting Diodes Using Nickel Oxide Hole Injection Layer. *Adv. Sci.* **2018**, *5*, 1801350.
(34) He, J.; Xiang, Y.; Zhang, F.; Lian, J.; Hu, R.; Zeng, P.; Song, J.; Qu, J. Improvement of Red Light Harvesting Ability and Open Circuit Voltage of Cu:NiO_x Based p-i-n Planar Perovskite Solar Cells Boosted by Cysteine Enhanced Interface Contact. *Nano Energy* **2018**, *45*, 471−479.
(35) Liu, S.; Hu, L.; Huang, S.; Zhang, W.; Ma, J.; Wang, J.; Guan, X.; Lin, C.-H.; Kim, J.; Wan, T.; Lei, Q.; Chu, D.; Wu, T. Enhancing the Efficiency and Stability of PbS Quantum Dot Solar Cells through Engineering an Ultrathin NiO Nanocrystalline Interlayer. *ACS Appl. Mater. Interfaces* **2020**, *12*, 46239−46246.
(36) Yusoff, A. R. B. M.; Gavim, A. E. X.; Macedo, A. G.; da Silva, W. J.; Schneider, F. K.; Teridi, M. A. M. High-Efficiency, Solution-Processable, Multilayer Triple Cation Perovskite Light-Emitting Diodes with Copper Sulfide−Gallium−Tin Oxide Hole Transport Layer and Aluminum-Zinc Oxide−Doped Cesium Electron Injection Layer. *Mater. Today Chem.* **2018**, *10*, 104−111.
(37) Wang, Z.; Luo, Z.; Zhao, C.; Guo, Q.; Wang, Y.; Wang, F.; Bian, X.; Alsaedi, A.; Hayat, T.; Tan, Z. a. Efficient and Stable Pure Green All-Inorganic Perovskite $CsPbBr_3$ Light-Emitting Diodes with a Solution-Processed NiO_x Interlayer. *J. Phys. Chem. C* **2017**, *121*, 28132−28138.
(38) Cao, F.; Wang, H.; Shen, P.; Li, X.; Zheng, Y.; Shang, Y.; Zhang, J.; Ning, Z.; Yang, X. High-Efficiency and Stable Quantum Dot Light-Emitting Diodes Enabled by a Solution-Processed Metal-Doped Nickel Oxide Hole Injection Interfacial Layer. *Adv. Funct. Mater.* **2017**, *27*, 1704278.
(39) Gao, X.; Chorover, J. Adsorption of Sodium Dodecyl Sulfate (SDS) at ZnSe and α-Fe_2O_3 Surfaces: Combining Infrared Spectroscopy and Batch Uptake Studies. *J. Colloid Interface Sci.* **2010**, *348*, 167−176.
(40) Wang, T.; Xie, M.; Abbasi, S.; Cheng, Z.; Liu, H.; Shen, W. High Efficiency Perovskite Solar Cells with Tailorable Surface Wettability by Surfactant. *J. Power Sources* **2020**, *448*, 227584.
(41) Okpalugo, T. I. T.; Papakonstantinou, P.; Murphy, H.; McLaughlin, J.; Brown, N. M. D. High resolution XPS characterization of chemical functionalised MWCNTs and SWCNTs. *Carbon* **2005**, *43*, 153−161.
(42) Roy, S.; Yue, C. Y. Surface Modification of COC Microfluidic Devices: A Comparative Study of Nitrogen Plasma Treatment and its Advantages Over Argon and Oxygen Plasma Treatments. *Plasma Processes Polym.* **2011**, *8*, 432−443.
(43) Wang, K.-C.; Shen, P.-S.; Li, M.-H.; Chen, S.; Lin, M.-W.; Chen, P.; Guo, T.-F. Low-Temperature Sputtered Nickel Oxide Compact Thin Film as Effective Electron Blocking Layer for Mesoscopic NiO/$CH_3NH_3PbI_3$ Perovskite Heterojunction Solar Cells. *ACS Appl. Mater. Interfaces* **2014**, *6*, 11851−11858.
(44) Conrad, J. R.; Radtke, J. L.; Dodd, R. A.; Worzala, F. J.; Tran, N. C. Plasma Source Ion-Implantation Technique for Surface Modification of Materials. *J. Appl. Phys.* **1987**, *62*, 4591.
(45) Hou, R.; Fang, X.; Li, L.; Li, S.; Song, W.; Xie, X.; Xie, Z.; Xu, W.; Pan, S.; Li, D.; Xiao, C.; Qin, G. G. Doping Si, Mg and Ca into GaN Based on Plasma Stimulated Room-Temperature Diffusion. *Appl. Phys. A* **2017**, *123*, 393.
(46) Wang, H.; Li, X.; Yuan, M.; Yang, X. Fast Postmoisture Treatment of Luminescent Perovskite Films for Efficient Light-Emitting Diodes. *Small* **2018**, *14*, 1703410.
(47) Kang, D.-H.; Kim, S.-G.; Kim, Y. C.; Han, I. T.; Jang, H. J.; Lee, J. Y.; Park, N.-G. $CsPbBr_3/CH_3NH_3PbCl_3$ Double Layer Enhances Efficiency and Lifetime of Perovskite Light-Emitting Diodes. *ACS Energy Lett.* **2020**, *5*, 2191−2199.
(48) Tian, J.; Xue, Q.; Tang, X.; Chen, Y.; Li, N.; Hu, Z.; Shi, T.; Wang, X.; Huang, F.; Brabec, C. J.; Yip, H. L.; Cao, Y. Dual Interfacial Design for Efficient $CsPbI_2Br$ Perovskite Solar Cells with Improved Photostability. *Adv. Mater.* **2019**, *31*, 1901152.
(49) Lee, S.; Jang, C. H.; Nguyen, T. L.; Kim, S. H.; Lee, K. M.; Chang, K.; Choi, S. S.; Kwak, S. K.; Woo, H. Y.; Song, M. H. Conjugated Polyelectrolytes as Multifunctional Passivating and Hole-Transporting Layers for Efficient Perovskite Light-Emitting Diodes. *Adv. Mater.* **2019**, *31*, 1900067.

https://dx.doi.org/10.1021/acsami.0c16139
ACS Appl. Mater. Interfaces 2020, 12, 53528−53536